Mon. Not. R. Astron. Soc. **276,** 353–371 (1995)

A deep optical imaging study of the nebular remnants of classical novae

A. J. Slavin,★ T. J. O'Brien★ and J. S. Dunlop†
Astrophysics Group, Liverpool John Moores University, Byrom Street, Liverpool L3 3AF

Accepted 1995 March 13. Received 1995 March 10; in original form 1994 December 15

ABSTRACT

An optical imaging study of old nova remnants has revealed previously unobserved features in the shells of 13 classical novae – DQ Her, FH Ser, HR Del, GK Per, V1500 Cyg, T Aur, V533 Her, NQ Vul, V476 Cyg, DK Lac, LV Vul, RW UMi and V450 Cyg. These data indicate a possible correlation between nova speed class and the ellipticity of the resulting remnants – those of faster novae tend to comprise randomly distributed clumps of ejecta superposed on spherically symmetric diffuse material, whilst slower novae produce more structured ellipsoidal remnants with at least one and sometimes several rings of enhanced emission. By measuring the extent of the resolved shells and combining this information with previously published ejection speeds, we use expansion parallax to estimate distances for the 13 novae. Whilst we are able to deduce new information about every nova, it is notable that these observations include the first detections of shells around the old novae V450 Cyg and NQ Vul, and that velocity-resolved images of FH Ser and DQ Her have enabled us to estimate their orbital inclinations. Our observations of DQ Her also show that the main ellipsoidal shell is constricted by three rings and surrounded by a faint halo; this halo contains long tails extending outwards from bright knots, perhaps indicating that during or after outburst a fast inner wind has broken through the fractured principal shell.

Key words: circumstellar matter – novae, cataclysmic variables.

1 INTRODUCTION

The eruption of a classical nova results in the ejection of $\sim 10^{-4}\,M_{\odot}$ of material at velocities of up to several thousand kilometres per second (Bode & Evans 1989). The study of this ejected material is important for broad areas of interest such as distance determination, the chemical evolution of the interstellar medium, the astrophysics of dust formation, and gas dynamics. It can also provide additional insight into otherwise unobservable processes that occur during the outburst itself. Our understanding of such mass ejection processes is relevant not only to novae, but also to other objects in which similar mechanisms may be at work, such as planetary nebulae and some supernovae. This paper represents the latest stage in a collaborative investigation of mass ejection in novae, combining theory with observations at a range of wavelengths (radio – Pavelin et al. 1993; Lloyd et al. 1993; submillimetre – Ivison et al. 1993; optical – Slavin, O'Brien & Dunlop 1994; ultraviolet – Evans et al. 1992; and X-ray – O'Brien, Lloyd & Bode 1994; Lloyd et al. 1992; O'Brien, Bode & Kahn 1992).

Given that every nova should be surrounded by an expanding cloud of ejecta, it is perhaps surprising that the literature contains few images of classical nova remnants; in fact only 26 of the 200 or so known classical novae have detected shells (Wade 1990). This is presumably a consequence of the rarity of survey observations [the only previous published work of this kind is by Cohen (1985, hereafter C85), Cohen & Rosenthal (1983, hereafter CR83) and Duerbeck (1987c)]. In order to exploit the full potential of the remnant phase it is necessary to have unambiguous images. Previous remnant detection has often relied on point-spread-function (PSF) comparison (e.g. V533 Her, LV Vul, DK Lac, RW UMi: CR83, C85) while the few archival images of varying quality are dispersed throughout the literature. We have therefore embarked upon a deep imaging survey of classical nova remnants using large telescopes combined with modern detectors. The first results, images of 13 objects, are presented in this paper. In virtually all cases these reveal previously unresolved structures.

★ e-mail: ajs, tob@starul.livjm.ac.uk
† Present address: Institute for Astronomy, University of Edinburgh, Blackford Hill, Edinburgh EH9 3HJ, UK.

In the following section we describe our observations. In Section 3 we present the images, describing and interpreting the main features seen in each object. In Section 4 we present evidence of a link between the speed class of a nova and the shape of its remnant. We also discuss the determination of distances from expansion parallax and derive such distance estimates from our data. We conclude with a brief summary of the main points of the paper.

2 OBSERVATIONS

Our target objects were selected either from the group of classical novae known to have extended material discussed by Wade (1990) or from the objects investigated with varying degrees of success by CR83 and C85. The targets also had to be observable from La Palma in the Canary Islands at the time of the observing run. The majority of the observations were made on 1993 September 9–11 with the 4.2-m William Herschel Telescope (WHT). The only other image presented in this paper was obtained three weeks prior to the WHT run on the 1.0-m Jacobus Kapteyn Telescope (JKT). Two separate instruments were used on the WHT: five of the 13 objects were observed using TAURUS 2 (an imaging Fabry–Perot interferometer: Unger et al. 1990) in imaging mode with the $f/2$ camera and the TEK1 CCD, giving an image scale of 0.58 arcsec per pixel, while seven of the targets were observed at the auxiliary port of the telescope with a binned EEV3 CCD, giving an image scale of 0.20 arcsec per pixel. The JKT observation was obtained with the GEC CCD camera mounted at the $f/15$ Cassegrain focus, giving an image scale of 0.32 arcsec per pixel.

Table 1 lists the effective central wavelength and width (FWHM) of the filters used, the band numbers employed later in the paper to identify various filters, and the total exposure times for each observation. A notable feature of the observations using the WHT/TAURUS 2 is that the 6560-Å filter was tilted to obtain small blueward shifts in its central wavelength. This provides some limited velocity resolution if we assume that either Hα 6563-Å emission dominates [N II] 6583-Å emission or vice versa. The 6560-Å filter was tilted by 7° and 10°, resulting in wavebands with effective central wavelengths of 6549 and 6537 Å respectively. Physically, the 7° tilted filter will be centred on Hα emission with velocity -640 km s^{-1}, while the 10° tilted filter will be centred on Hα emission with velocity -1190 km s^{-1}. The bandwidth of the tilted filter will increase and the overall transmission will decrease although these new characteristics are not well determined (Unger et al. 1988). Also, the [N II] 6583-Å filter will be centred on Hα emission with velocity $+1143$ km s^{-1}. The bandwidth of the untilted 6560-Å filter gives an effective velocity coverage of ± 400 km s^{-1}. As a result of time constraints this procedure was only used in observations of four of the brightest and most extended remnants. In addition to the images presented here, we also observed two of the novae (DQ Her and GK Per) using TAURUS 2 in its full Fabry–Perot mode. The results of these observations will be presented in a separate paper.

Flat-fields for each of the telescope, filter and chip combinations were obtained by observing blank areas of sky at dusk. Multiple bias frames were obtained and co-added to produce master-bias frames for each chip. Basic data reduction was performed using the CCDPACK software package within the Starlink suite of routines. During the WHT run the atmospheric seeing over the three nights of the observations was 0.9 ± 0.2 arcsec (this value is an average of 21 seeing estimates made throughout the run). The seeing for the JKT observation, where estimates were taken after each exposure, was also 0.9 arcsec.

3 THE IMAGES

3.1 DQ Herculis

3.1.1 Background

The moderately fast nova DQ Her (Nova Herculis 1934) reached a maximum visual magnitude of 1.4 and declined with a t_3 (the time taken to decline 3 mag from peak bright-

Table 1. Details of the integration times (in seconds) of the observations presented in this paper. The band numbers refer to particular telescope and/or filter combinations. The effective central wavelength and full widths at half-maximum are given in ångstroms for each filter. The instrumental setup used in each observation is also noted (TAURUS – TAURUS 2 on the WHT; Aux. port – the auxiliary port CCD camera on the WHT; JKT – the CCD camera on the JKT). Band 3 and band 4 represent the wavebands obtained by tilting the band 5 filter by 10° and 7° respectively. Those times marked with an asterisk are total exposure times obtained by co-adding frames; see Section 3 for further details.

Band	1	2	3	4	5	6	7	8	9
Filter	4872/15	5010/18	6537/>17 (6560/10°)	6549/>17 (6560/7°)	6560/17	6569/17	6588/18	6608/19	5012/50
Instrument	TAURUS	TAURUS	TAURUS	TAURUS	TAURUS	Aux. port	TAURUS	TAURUS	JKT
DQ Her	300		300	300	600*		300	300	
FH Ser			300	300	300		300	300	
HR Del			60	60	60		60	60	1800*
GK Per		300			60		300	60	
V1500 Cyg						1200			
T Aur					1320*				
V533 Her						1800*			
NQ Vul						1800*			
V476 Cyg						900			
DK Lac						900			
LV Vul						900			
RW UMi						600			
V450 Cyg						1200			

ness) of 94 d. It has a quiescent visual magnitude of 14.7 (see Duerbeck 1987b and Bode & Evans 1989 for comprehensive data bases). The light curve was notable for the great minimum which occurred between 99 and 200 d after outburst. This dip in the optical light is thought to result from obscuration by dust and is a characteristic of the dust-forming class of novae of which DQ Her is the prototype. One of the most recent images of the resolved nebular remnant (taken through a broad Hα filter by Duerbeck and Seitter and published by Martin 1989) shows an elliptical shell with pronounced condensations. Notably, the shell is crossed by an obvious band in the equatorial plane and two further 'tropical' bands towards the poles of the shell. DQ Her was discovered to be an eclipsing binary system by Walker (1956), with the orbital inclination estimated to be greater than 80°. Martin (1989) derived a distance of 485 ± 50 pc from expansion parallax. This system is also the archetype of the intermediate polar class of magnetic cataclysmic variables and contains a white dwarf with a magnetic field strength of $\sim 6 \times 10^5$ G (Lamb & Patterson 1983).

3.1.2 *Results*

The remnant of DQ Her was imaged for 300 s in wavebands 1, 3, 4, 7 and 8 and for 600 s (two 300-s exposures) in band 5, giving a wavelength coverage from approximately 4870 to 6610 Å. The band 8 image is not shown in this paper as no extended nebula was detected. The object 4 arcsec south-east of the central object in all the images of DQ Her is probably a field star as it appears at the same location in all observations ranging from archival photographs to the present images. The results are shown in Fig. 1.

The image in band 1, the shortest waveband used, shows an oval remnant with approximate dimensions 35×24 arcsec^2, Fig. 1(a). These dimensions represent the extent of the nebular emission visible above the noise. The brightest emission is confined to a shell of very clumpy material with approximate dimensions 23×16 arcsec^2. The major axis has position angle (PA) ~ 135° (measured anticlockwise from north). The most luminous and apparently broadest portions of the shell are at the extremes of the major axis. The shell gradually reduces in thickness and surface brightness towards the minor axis where there is only diffuse emission with a few faint blobs. The central regions of the remnant also contain structure; in particular there is a thin arc of emission across the minor axis of the shell, with its central portion about 1 arcsec north-west of the central source. Slices across the bright sections of the shell at the extremities of the major axis and parallel to the minor axis show that the emission at the north-western end is composed of at least five distinct sources. A similar slice in the south-east shows fewer sources divided into two regions of emission.

The image of the remnant of DQ Her through band 3 is shown in Fig. 1(b). As in band 1 the remnant is oval in shape but in this case with approximate dimensions 29×21 arcsec^2. There is also a concentration of material in a shell. On top of the overall diffuse emission there are thin strips of greater surface brightness about 6 arcsec from, and parallel to, the minor axis. These strips do not appear to extend to the outer south-western edge of the nebula.

The image through band 4 is shown in Fig. 1(c). The remnant consists of a well-defined oval, inhomogeneous shell surrounding the central object. The total extent is approximately 41×28 arcsec^2. The two bands of enhanced emission parallel to the minor axis which were visible in Fig. 1(b) can also be seen in Fig. 1(c). The brighter of the bands is in the south-eastern half of the remnant. The brightest portions of the shell are again at the extremes of the major axis. The image shows five separate sources at the north-western end and four sources at the south-eastern end. The brightest of these sources are elongated radially and appear to have 'tails' extending outwards which originate in the bright blobs. The longest of these tails, at a PA of ~ 320°, extends ~ 10 arcsec from the progenitor blob. The bright shell has approximate dimensions 24×16 arcsec^2.

The image in Fig. 1(d) was produced by co-adding two 300-s exposures of DQ Her through waveband 5. This image shows a complete shell with emission from many distinct blobs, the brightest of which are concentrated at the extremes of the major axis. At the ends of the minor axis the shell exhibits cusps where the emission arcs inwards. The central region of the remnant appears to have fainter bands of emission running parallel to, and along, the minor axis. Cusps are also evident in the outer shell at the points where the bands parallel to the minor axis meet the shell. Tails extending up to ~ 20 arcsec in length, emanating from at least six of the bright blobs, can be seen at either end of the major axis. Similar features can also be seen at the four protruding regions between the cusps close to the extremes of the minor axis, although at these points the emitting regions and the associated tails are much wider and appear to be less extended. The overall nebula extends to approximately 47×29 arcsec^2 before fading into the noise. The shell of bright emission has approximate dimensions 23×17 arcsec^2.

The image of the remnant of DQ Her through waveband 7 is shown in Fig. 1(e). The remnant has dimensions 38×23 arcsec^2. There is no complete bright shell as in Fig. 1(d), for example. In fact, the emission is concentrated in clumpy 'caps' at the ends of the major axis, and in three narrow bands aligned with the minor axis and arcing slightly to the north-west. The middle band is the most distinct and is brightest at its extremes.

3.1.3 *Image processing*

It is clear that, if the elliptical halo could be removed in some way, the extent and morphology of the tails detected in waveband 5 (Fig. 1d) could be more easily determined. In Fig. 2 we present the result of an attempt to achieve this by decomposing the nebula around DQ Her (Figs 1d and 2a) into two components, one of which contains all (and only) those features that possess a basically elliptical symmetry. This image (shown in Fig. 2b) was produced as follows. First, the centroid, position angle and axial ratio of the elliptical shell were determined in an automated way using moment analysis (see Section 4.2). These parameters were then used to fix the shape and orientation of elliptical annuli of width 1 pixel. Within each such annulus each pixel was replaced by the median value of all pixels within a 25° sector centred on itself. The result is a synthetic object with broad elliptical symmetry but which is allowed smoothly varying structure on angular scales $\geq 25°$. The result of subtracting this 'elliptical' object from the original image is shown in Fig. 2(c),

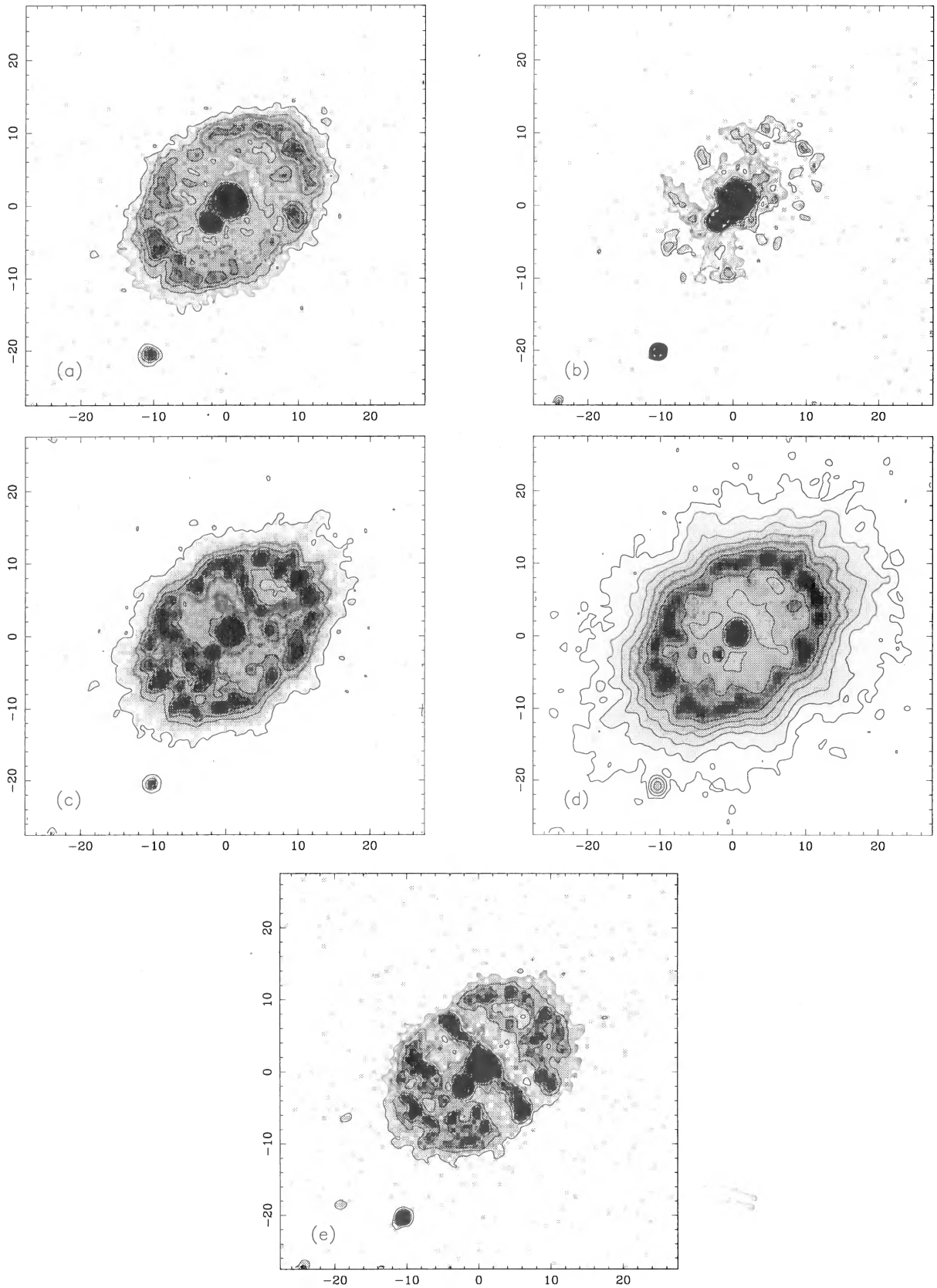

Figure 1. Narrow-band CCD images of the remnant of DQ Her. In all five plots, north is up, east is to the left, the bottom contour has been set at 2σ above the background and axes are marked in arcsec. The images are: (a) band 1 (Hβ) with 3σ contour intervals; (b) band 3 (tilted Hα, 6537-Å effective central wavelength) with 1σ contour intervals; (c) band 4 (tilted Hα, 6549-Å effective central wavelength) with 8σ contour intervals; (d) band 5 (Hα rest-frame) with 5σ contour intervals; and (e) band 7 ([N II] rest-frame) with 3σ contour intervals. See Section 3.1 for further details.

and it can be seen that, as desired, we have effectively 'flat-fielded' out the elliptical nebula to leave a residual image containing only the tails. The properties of the tails can now be discerned much more easily than in Fig. 1(d). First, the tails can now clearly be seen to extend up to ~20 arcsec from their points of origin in the main shell. Secondly, the image displays striking (non-elliptical) symmetry, with five tails extending out from each of the poles, and two from either side of the minor axis. Thirdly, as we suggest in the previous section, the tails at the poles are markedly clearer than the more diffuse tails in the orthogonal plane.

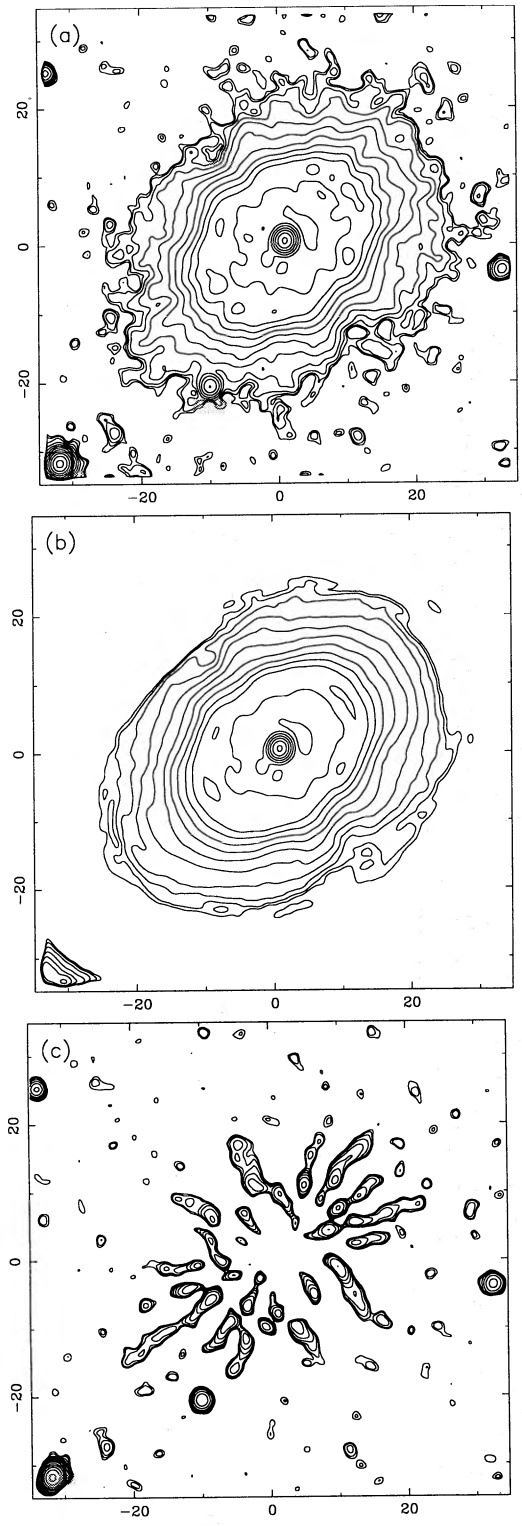

3.1.4 *Interpretation*

The series of images in Figs 1(a)–(e) indicates that the nebular remnant of DQ Her takes the form of an ellipsoidal shell constricted by three bands of enhanced emission. Examination of the curvature of these bands, assuming that they are intrinsically circular, indicates that the shell is tilted at $9° \pm 4°$ to the line of sight with the north-western quadrant tilted towards us. If we further assume that the equatorial ring around the waist of the shell lies in the orbital plane of the binary system, then an orbital inclination of ~81° is deduced. DQ Her is an eclipsing binary, implying that the equatorial plane does indeed lie in the orbital plane. The faint halo and long tails of emission particularly evident in band 5 (the deep Hα rest frame: Fig. 2c) are suggestive of the effects of an inner fast wind breaking through a dense clumpy shell either during or some time after the outburst (e.g. Dyson, Hartquist & Biro 1993 for tails in planetary nebulae and Duerbeck 1987c for the southern nova. From studying the spectral line history in the first 100 d after outburst, Martin (1989) concluded that there was a fast-moving wind interior to the principal shell and this wind had twice the shell's velocity. Such an interacting winds model has been used to explain the X-ray emission observed early in the outburst of the classical nova V838 Her (O'Brien, Lloyd & Bode 1994). Alternatively, the tails may represent regions of the halo which are shadowed from the central photoionizing radiation field by the dense clumps.

3.2 FH Serpentis

3.2.1 *Background*

FH Ser (Nova Serpentis 1970) brightened in outburst from a quiescent visual magnitude of 14.5 to peak at 4.5. The maximum was followed by a moderately fast decline with a t_3 of 62 d. From spectroscopic evidence, Hutchings (1972) suggested that the ejected material consisted of three components: two oppositely directed polar caps, a less dense equatorial ring, and a rapidly moving spherically symmetric shell from which diffuse emission arises. Duerbeck (1992) produced the first image of the resolved remnant of FH Ser, in which a shell of radius 2.7 arcsec was seen with what he suggested was an equatorial band of enhanced emission. From this image, he estimated an orbital inclination of 58° and a distance of 850 pc.

Figure 2. The result of the image decomposition of the band 5 image of DQ Her which was presented in Fig. 1(d). The raw image is reproduced in (a) after a 2-pixel smooth (although with a somewhat larger field of view), and this time displayed with successive contours separated by a factor of 2 in flux (the height of the bottom contour is the same as the 1σ noise level in the raw unsmoothed image). In (b) we show the elliptically symmetric median-filtered version of (a) contoured in exactly the same way. The result of subtracting frame (b) from (a) is shown in (c) (again contoured according to the same recipe). This third image emphasizes features that do not possess elliptical symmetry on angular scales of less than 25°, and hence displays the extended tails to their best effect. See Section 3.1.3 for further details.

3.2.2 *Results*

The remnant of FH Ser was observed in wavebands 3, 4, 5, 7 and 8 with 300-s exposures in each band, giving wavelength coverage from approximately 6530 to 6608 Å. Structure is visible in all but the reddest image where there is no evidence of extended material. About 4 arcsec from the central star at a PA of about 130°, there is a faint, probably stellar, feature which is seen in all the images.

In band 3, Fig. 3(a), the central object of FH Ser is surrounded by a region of diffuse emission extending out to a radius of ~ 5 arcsec. Slices along the north–south axis show that the emission peaks at a radius of approximately 2.5 arcsec. There is also a crescent of enhanced emission extending the length of the north–south axis in the western hemisphere, about 1 arcsec from the central source at closest approach. A slice along the east–west axis shows a shoulder of emission on the eastern side of the central object.

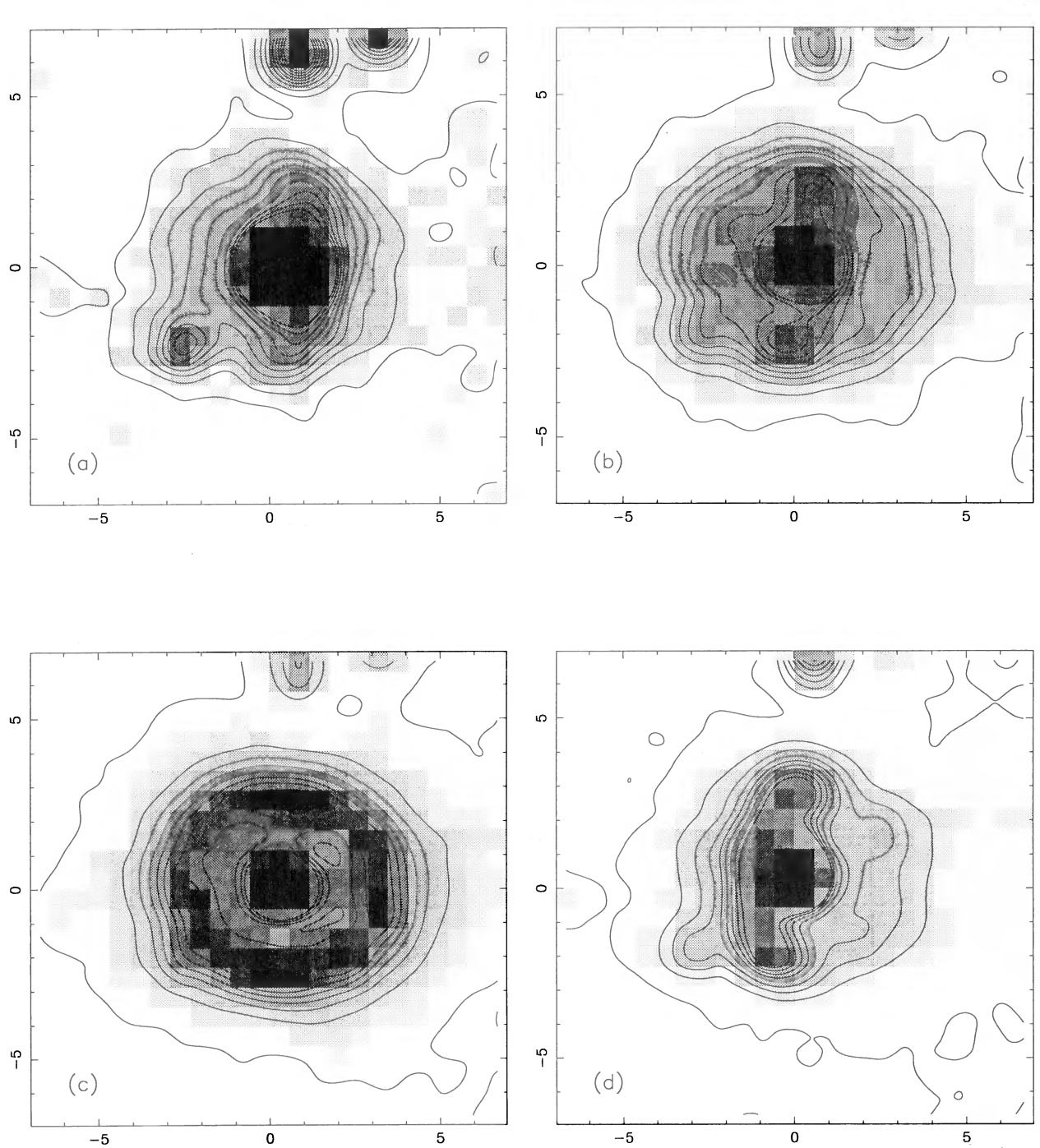

Figure 3. Narrow-band CCD images of the remnant of FH Ser. In all four plots, north is up, east is to the left and axes are marked in arcsec. The bottom contour level in each frame is set at 2σ above the background. The frames contain the following images: (a) band 3 (tilted Hα, 6537-Å effective central wavelength) with 3σ contour intervals; (b) band 4 (tilted Hα, 6549-Å effective central wavelength) with 2σ contour intervals; (c) band 5 (Hα rest-frame) with 14σ contour intervals; and (d) band 7 ([N II] rest-frame) with 2σ contour intervals. See Section 3.2 for further details.

The image in band 4, Fig. 3(b), again shows a crescent at the same position, although of somewhat greater surface brightness and ~0.6 arcsec wide. The brightest portions of the crescent are at its northern and southern extremes; as with the arc in Fig. 3(a) this is suggestive of the effects of limb brightening. The remnant has approximate overall dimensions of 11.5×10.5 arcsec^2, the elongation being along the east–west axis. Slices across the remnant indicate that the brightest nebular emission, apart from the crescent, originates in a ring. The eastern half of the ring has a radius of ~3.0 arcsec, the western half a radius of ~2.5 arcsec.

In band 5, Fig. 3(c), the remnant takes the form of a slightly elliptical, clumpy ring with a radius of about 3 arcsec. The ring itself is 1.5 arcsec in width and is filled and surrounded by a diffuse nebula which extends at least 6 arcsec from the central star. There is no visible band of emission along the north–south axis as in the previous two frames.

The image in band 7, Fig. 3(d), the longest waveband presented here and therefore tending to emphasize material with the largest redshift, again shows a crescent but now in the eastern half of the remnant and curving in the opposite sense to that seen in Figs 3(a) and (b). The 1 arcsec wide crescent extends approximately 6 arcsec along the north–south axis. As with the other bands there is an extended region of diffuse emission which is slightly elongated in the east–west direction.

3.2.3 *Interpretation*

The remnant of FH Ser appears to consist of an expanding shell of material with a radius of ~3.5 arcsec. The material in band 5 represents limb-brightened rest-frame Hα emission from this shell and therefore has the appearance of an approximately circular ring. The crescents of emission seen to the west of the central object in bands 3 and 4 and to the east in band 7 can be interpreted as a ring of enhanced emission around the waist of the remnant, the western edge approaching the observer while the eastern edge is receding. Examination of the curvature of these crescents indicates that the equatorial plane is tilted at $32° \pm 14°$ to the line of sight, implying an orbital inclination of ~58°, in agreement with the estimate of Duerbeck (1992). It appears that, as with DQ Her, the bright shell is surrounded by diffuse emission, perhaps representing material ejected at higher speeds during outburst. In fact, there is spectroscopic evidence (Friedjung 1989) that, during the first 60 d after outburst, mass was ejected at several different velocities. In particular, there was an absorption-line system with a velocity of around 700 km s^{-1}, and another with velocity increasing over this period from about 1300 to 1900 km s^{-1}. We do not resolve any extended tails in the halo around FH Ser, probably as a result of the rather limited extent of the nebula in comparison with that of DQ Her.

3.3 HR Delphini

3.3.1 *Background*

HR Del (Nova Delphini 1967) was an unusually slow nova with a t_3 of greater than 230 d. It brightened at outburst from a visual magnitude of 11.9 to peak at 3.8. The first photographic image of the resolved ejecta (Kohoutek 1981) revealed an oval-shaped remnant. The first published CCD images of the remnant (Slavin et al. 1994, hereafter SOD94) showed an ellipsoidal object in the light of [O III] and a more circular object in the light of Hα/[N II]. A similar wavelength-dependent morphology was seen in early photographs of DQ Her (Baade 1940). Deconvolution of the SOD94 images using the maximum entropy method (MEM) and a CLEAN algorithm revealed a bipolar morphology for the [O III] image and a more ring-like structure for the Hα/[N II] image, suggesting that the bipolar blob/equatorial ring model proposed by several authors (e.g. Hutchings 1972; Solf 1983) from the evidence of high-resolution spectroscopy is appropriate for this object. Solf (1983), using a spatio-kinematic model, suggested that the polar axis is inclined at an angle of 38° with respect to the line of sight, and also estimated a distance of 1.15 kpc. This object was observed with the pre-COSTAR *Hubble Space Telescope* (Paresce 1993), but unfortunately this unpublished image stored in the data archive is saturated.

3.3.2 *Results*

The remnant of HR Del was observed for 60 s in each of the bands 3, 4, 5, 7 and 8; it was also observed through an [O III] filter with the JKT CCD camera, band 9 giving an approximate wavelength coverage of 5012 to 6608 Å. The image through the band 8 filter revealed no evidence of extended material. The other images are shown in Figs 4(a)–(e) respectively.

Band 3, the most blueward of the HR Del Hα observations, shows a rectangular-shaped remnant with approximate dimensions 11×9 arcsec^2, the major axis lying from the north-east to south-west, with the bulk of the emission lying to the south-west of the central star (Fig. 4a). This extended material is not completely resolved from the bright central system; slices show broad shoulders of emission superimposed on a stellar profile. The radius of the bulk of material can, however, be obtained by estimating the position of the peak of the shoulder. Slices across the frame from north-east to south-west show that the remnant is extended up to ~6 arcsec either side of the central source. The peak brightness in the south-westerly direction is five times brighter than in the north-easterly direction. In this case it appears that the emission peaks at ~3.5 arcsec on either side of the central star. In the orthogonal direction there is no clear shoulder in the profile, although it is more extended than one would expect from a stellar PSF. A slice parallel to the minor axis across the bright extended material in the south-west does not reveal any obvious structure.

Band 4, Fig. 4(b), shows a rectangular-shaped remnant with approximate dimensions 11.5×8.5 arcsec^2. As before, the remnant is asymmetric with the bulk of the extended emission appearing to be in the south-west. The emission in the north-east is brighter than its band 3 counterpart, the ratio of the peak surface brightness of the opposing halves in this case being approximately 3:1. Again slices along the north-east/south-west axis reveal that the brightness peaks are equidistant from the central object at ~3 arcsec. A slice along the north-west/south-east axis shows that there is extended material at a distance of 2 arcsec either side of the centre. These features have approximately the same surface brightness. The feature in the south-western quadrant

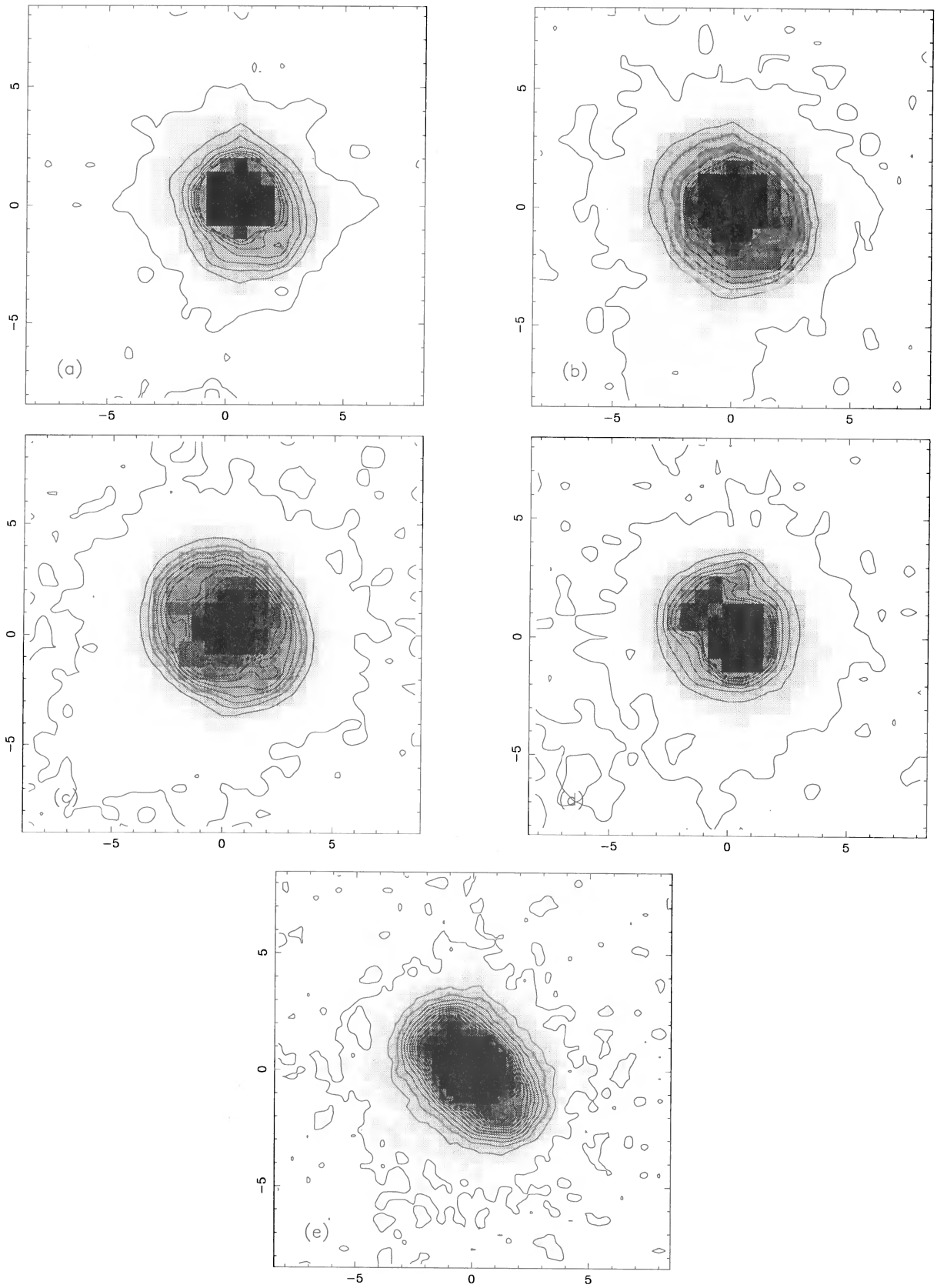

Figure 4. Narrow-band CCD images of the remnant of HR Del. In all five plots, north is up, east is to the left and axes are marked in arcsec. The bottom contour level in each frame is set at 2σ. The frames contain the following images: (a) band 3 (tilted Hα, 6537-Å effective central wavelength) with 11σ contour intevals; (b) band 4 (tilted Hα, 6549-Å effective central wavelength) with 33σ contour intervals; (c) band 5 (Hα rest-frame) with 57σ contour intevals; (d) band 7 ([N II] rest-frame) with 36σ contour intervals; and (e) band 9 ([O III] rest-frame) with 8σ contour intervals. See Section 3.3 for further details.

appears to form a 'hook' of emission, perhaps representing part of a ring, emerging from the southerly portion of the PSF of the central star and curving round to the south-west. Note that extension of the 2σ contour to the south-south-east indicates the presence of a faint ghost feature.

The remnant in band 5, the Hα rest frame, Fig. 4(c), has approximate dimensions 12×9 arcsec^2. It again appears approximately rectangular in shape although somewhat rounded at the north-east and south-west extremes. Slices show the nebular emission peaking at a radius of ~ 3 and ~ 2 arcsec along the major and minor axes respectively, with approximately equal surface brightness. Slices along the north-south and east-west axes show emission peaked at the same radius but of slightly lower surface brightness. The emission is clearly enhanced to the north-west and south-east of the central star, and some structure is visible in the nebula to the north-east and south-west. As with Fig. 4(b), slight ghosting is visible to the south-east.

In band 7, Fig. 4(d), the remnant morphology is almost a mirror image of that in band 3. The remnant has approximate dimensions of 9×8 arcsec^2 with the bulk of the emission concentrated in the north-eastern section. The emission in this region peaks at a distance of ~ 2.5 arcsec from the central object and is approximately 10 times brighter than the extended emission on the opposite side which peaks at the same radius. There is evidence of extended emission along the minor axis, the peak of which is also at a radius of ~ 2.5 arcsec. The emission in the north-east takes the form of a bar or possibly two blobs extended in a direction orthogonal to that of the major axis of the remnant.

HR Del was also observed using the JKT through an [O III] filter, Fig. 4(e), band 9 in Table 1. To avoid saturation, and obtain sufficient signal, the image was produced by co-adding two frames with a total integration time of 1800 s. Slices across the image indicate a morphology that differs from the wavebands above. A complete ring of emission is not seen but bright enhancements are observed ~ 2.5 arcsec away from the central object along the major axis. Slices across these enhancements indicate that they are formed from two 'blobs' in the north-eastern quadrant and by only one more extended component in the south-western quadrant. The features in the opposing quadrants appear to replicate those seen in bands 4 and 7 (Figs 4b and d). The slices also indicate that the positions of the enhancements in bands 4, 7, and 9 are co-spatial to within about 0.5 arcsec.

3.3.3 *Interpretation*

The simplest interpretation of the images presented above is to assume that the remnant of HR Del is an expanding ellipsoidal shell of predominantly Hα emission, the band 5 image, Fig. 4(c), representing the rest wavelength. The slices suggest that the remnant consists of a complete elliptical ring with enhanced emission along the major and minor axes. Fig. 4(c) also indicates that, as with DQ Her and FH Ser, the waist of the shell is encircled by an equatorial band of enhanced emission. The brightest sections of the elliptical ring are at radii of ~ 3 arcsec along the major axis and ~ 2 arcsec along the minor axis. The antisymmetric images in Figs 4(a) and (d) indicate that the north-eastern end of the remnant is tilted away from the observer. Any Hα emission seen in these frames would have line-of-sight velocities of at least -400 and $+200$ km s^{-1} respectively. The fact that emission with similar positive and negative velocities is seen either side of the central source indicates further that this tilt is closer to 45° than to either 0° or 90°. The lack of substantial emission along the minor axis in these bands suggests that the emission in this plane is of a lower velocity than along the major axis or is in the plane of the sky, a feature consistent with an ellipsoidal geometry and a prolate shell composed of fast-moving polar-directed blobs or rings and a slower-moving equatorial ring. The [O III] emission appears to replicate that of the Hα, at least along the major axis. As discussed in SOD94 the reason for the lack of [O III] emission along the minor axis, in comparison with that seen in Hα or [N II], is not clear but could be the result of either spatial abundance anomalies or differing physical conditions across the nebula.

These new images also indicate that the deconvolution employed by SOD94 on images taken in poorer seeing conditions gave the correct morphology. In particular, Fig. 4(d) appears to be in broad agreement with the deconvolved images, which suggests that the material at either end of the major axis is concentrated in two blobs.

3.4 GK Persei

3.4.1 *Background*

GK Per (Nova Persei 1901), the first bright nova of the twentieth century, peaked at a visual magnitude of 0.2 and declined rapidly with a t_3 of 13 d, classifying it as a very fast nova. The central object is now at a quiescent visual magnitude of 13.1 although it has occasional dwarf nova outbursts of amplitude around 3 mag. The expanding nebulosity was first detected photographically by Perrine (1902), and its expansion and development have been closely followed ever since (see Seaquist et al. 1989 for a detailed description). It has been suggested that the morphology and ionization of the shell are a result of the interaction of the nova ejecta with its own 'fossil' planetary nebula (Bode, Seaquist & Evans 1987; although Dougherty et al., in preparation, suggest that the material extended on scales of more than 30 arcmin originates from the secondary, and was ejected by the white dwarf long after the planetary nebula phase). The widely accepted distance for this object is 470 pc (McLaughlin 1960). The white dwarf in the GK Per central system is a hard X-ray-emitting source and is thought to have a strong magnetic field which Bianchini & Sabbadin (1983) estimated to be 5×10^5 G. The orbital inclination of the binary system has been estimated, from a correlation between emission-line widths and accretion disc inclination, to be $\sim 75°$ (Warner 1986).

3.4.2 *Results*

The images of GK Per in Figs 5(a)–(d) show the remnant through bands 2, 5, 7 and 8, a wavelength coverage of approximately 5010 to 6608 Å.

Fig. 5(a), the [O III] image of GK Per, shows a 'box-like' remnant with approximate dimensions 102×83 arcsec^2 with the major axis oriented at PA $\sim 120°$. Three sides of the remnant, in the north-eastern, north-western and south-

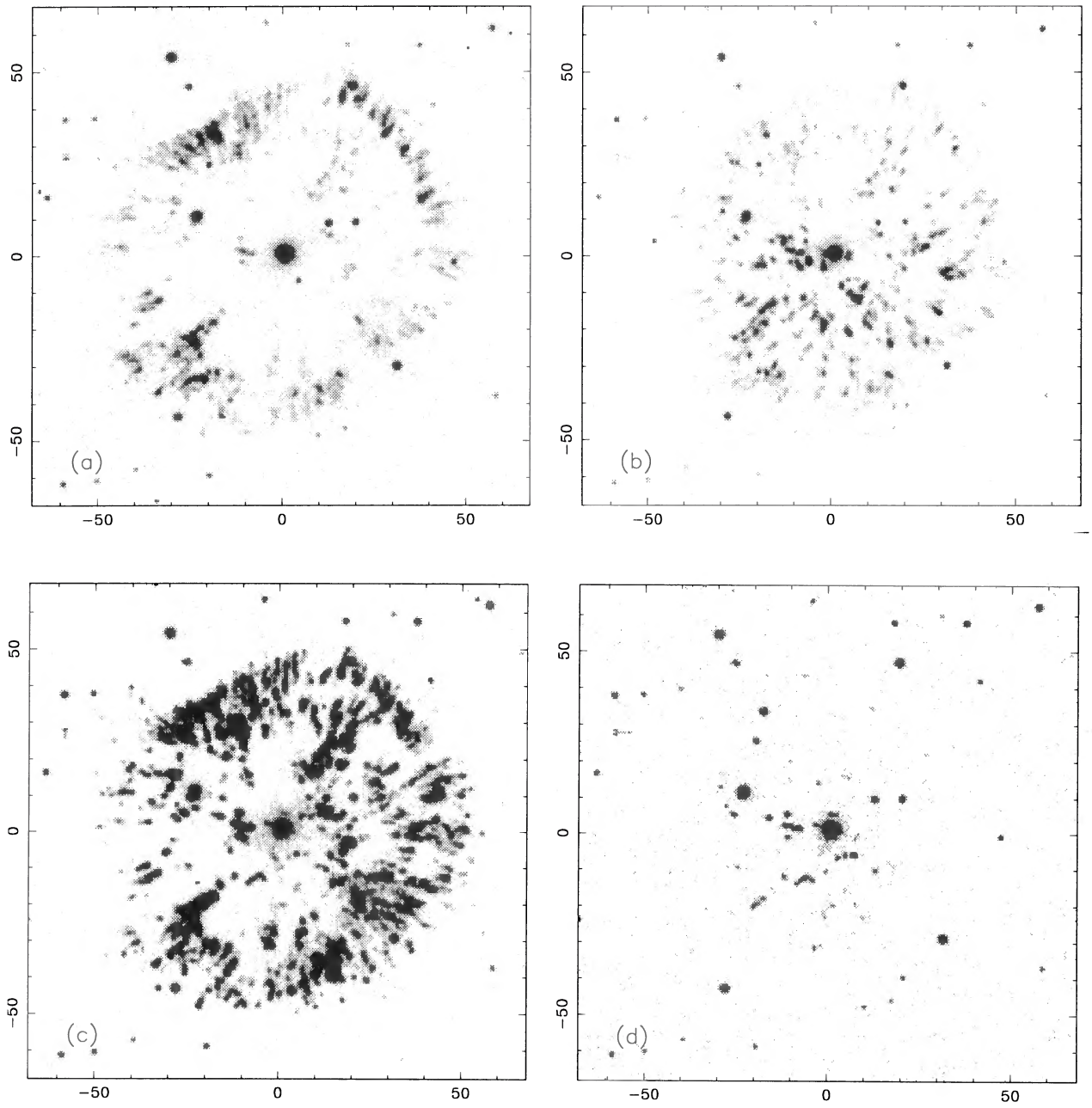

Figure 5. Narrow-band CCD images of the remnant of GK Per. In all four plots, north is up, east is to the left and axes are marked in arcsec. The four frames contain the following images: (a) band 2 ([O III]); (b) band 5 (Hα rest-frame); (c) band 7 ([N II] rest-frame); and (d) band 8 (central wavelength 6613 Å). See Section 3.4 for further details.

western quadrants, appear to be almost square on to the central object, forming three sides of a rectangle. The south-eastern quadrant is markedly different from the other three, forming an arc of emission from PA ~ 58° through to PA ~ 121°. The inhomogeneous shell itself consists of elongated 'blobs' of emission with various widths and surface brightnesses, directed radially in the general direction of the central object. There is a particularly bright, flattened portion of the shell at PA ~ 35°.

Fig. 5(b) shows the results of a 60-s exposure in band 5, the Hα rest frame. The remnant is almost circular but shows asymmetry in the distribution of emission, with the bulk of the bright emission concentrated in the southern half. The knots again appear elongated, mostly towards the central object, although in the brightest portion of the shell they are not radial but in fact give the impression of a 'blister' expanding from the main shell. The remnant extends to about 100×87 arcsec^2, the major axis lying approximately south-east to north-west.

The image of GK Per obtained from a 300-s exposure through the [N II] filter, band 7, is shown in Fig. 5(c). The remnant has approximate dimensions 103×90 arcsec^2, the major axis oriented from south-east to north-west. The remnant again appears to be three quarters of a rectangle

with an arc in the south-eastern quadrant, although the edge of the emission in the four quadrants is less well-defined than in the band 2 image. There is a 'hole' in the eastern edge of the shell with some indication that strands and knots of emission in the east-north-east extend out to ~15 arcsec past the outer edge of the main shell. As with the other bands these blobs are generally radially elongated, with, in several cases, the ones at the outer edges of the shell having an outer associated faint blob.

The image of GK Per in band 8, Fig. 5(d), central wavelength of 6608 Å, shows very little structure with only a few regions of emission within approximately 20 arcsec of the central object. The largest of these blobs are at PA ~80° and PA ~150° at distances of about 11 and 16 arcsec from the centre.

3.4.3 *Interpretation*

Archival [N II]/Hα images of GK Per from 1917 to 1984 (e.g. Seaquist et al. 1989) have shown an asymmetric remnant with the brightest portion of the nebula in the south-western quadrant. This bright emission is thought to result from the interaction of the expanding shell with some dense circumstellar medium. The [N II] image presented in Fig. 5(c) shows that the region of highest surface brightness is now concentrated in the north-eastern quadrant where a cone of bright knots of emission subtends an angle of ~80° to the central object. This region of the expanding nebula bears a remarkable resemblance to the interaction in the opposite quadrant circa 1949 (see Seaquist et al. 1989). We can infer from the 'flatness' of the outer boundary of the shell in this region that the new emission is the result of a similar interaction. The [O III] images of these two opposing quadrants suggest that the two regions have different physical conditions. Archival images have always shown a lack of [O III] emission in the south-western interaction region which Seaquist et al. suggested was a result of suppression of emission in the low-velocity post-shock region. This behaviour is not as apparent in these images of the north-eastern quadrant where the [O III] emission has a similar structure to the [N II].

If we assume that the [N II] emission dominates the Hα (Seaquist et al. 1989 suggest that the [N II] is at least 20 times as strong as the Hα), then features picked out in band 5, Fig. 5(b), are likely to be due to [N II] emission with a radial velocity of at least -300 km s^{-1}. Fig. 5(b) shows that the south-eastern quadrant of the shell has bright knots of emission which are not seen in Fig. 5(c), the rest wavelength [N II] image. The extremely redshifted emission would be seen in Fig. 5(d). The changes in morphology in these three bands could be a result of the whole shell being tilted at some angle to the line of sight. Alternatively, it may be that the ejecta in the south-eastern region have 'burst out' from a high- to a low-density environment. This certainly appears to be the case in the eastern 'hole' and may also explain the blister-like appearance of a portion of the south-eastern quadrant of the shell.

3.5 V1500 Cygni

3.5.1 *Background*

V1500 Cyg (Nova Cygni 1975) is a well-studied very fast nova with a t_3 of 3.6 d. It brightened from below twenty-first magnitude to peak at a visual magnitude of 1.85, making it one of the brightest and fastest known novae. Becker & Duerbeck (1980) were the first to image the remnant and with the use of image-restoration techniques suggested that the shell was asymmetric with enhanced emission in the north-western quadrant. They derived a distance of 1350 pc from expansion parallax. A later image (Wade et al. 1990) showed, after PSF subtraction, a roughly circular shell with knots of increased brightness at three different position angles: 31°, 115° and 287°, the last of which was coincident with the Becker & Duerbeck knot of enhanced emission. A revised distance of 1800 ± 200 pc was estimated. V1500 Cyg is another classical nova system thought to contain a strongly magnetized white dwarf (Stockman, Schmidt & Lamb 1988).

3.5.2 *Results*

Fig. 6(a) is an image of V1500 Cyg taken through the Hα, band 6, filter with a 1200-s integration. It shows approximately circular diffuse emission with several enhancements in brightness, apparently scattered randomly across the face of the nebula. The four most prominent enhancements are at position angles (measured anticlockwise from north) 20°, 130°, 270° and 306° at distances from the centre of approximately 2.5, 2.9, 3.5 and 3.6 arcsec respectively. The enhancement at 130° is the brightest and most elongated and extends across to the central object. Slices through the nebula at eight different position angles show that the surface brightness of the diffuse nebula drops close to the star but increases to a peak at a radius of about 3 arcsec, before dropping away again into the noise by about 5 arcsec.

3.5.3 *Interpretation*

There is no obvious symmetry or organized structure in the remnant of V1500 Cyg. The remnant profile, as observed from the slices, implies a ring of material with a radius of ~3 arcsec presumably representing the main expanding shell. Hutchings & McCall (1977) attempted to model this remnant using bipolar blobs and an equatorial ring expanding radially at 660 and 720 km s^{-1} respectively. This was based on the four-peaked emission-line structure seen within a few days of maximum light. If a distance of 1350 pc is assumed then the brightest component of the shell must have an average velocity of at least 1600 km s^{-1}. If correct, their proposed model and our assumed distance would have produced symmetric features at radii of ~1 arcsec in the current image. It seems likely that the nova ejecta clumped fairly soon after outburst and that the peaks in the line profile can be associated with individual blobs that we see in our present-epoch image – see Section 4.1. The most obvious feature of the remnant of V1500 Cyg is its clumpiness. GK Per is much closer than V1500 Cyg and much older, and is therefore expected to be rather better resolved. If the image of the remnant of GK Per, Fig. 4(d), is degraded to the same quality as that of V1500 Cyg then it too displays a tendency to clump into typically four to six main regions of emission. However, in GK Per we are able to see that each clump is itself composed of many smaller blobs and radial features.

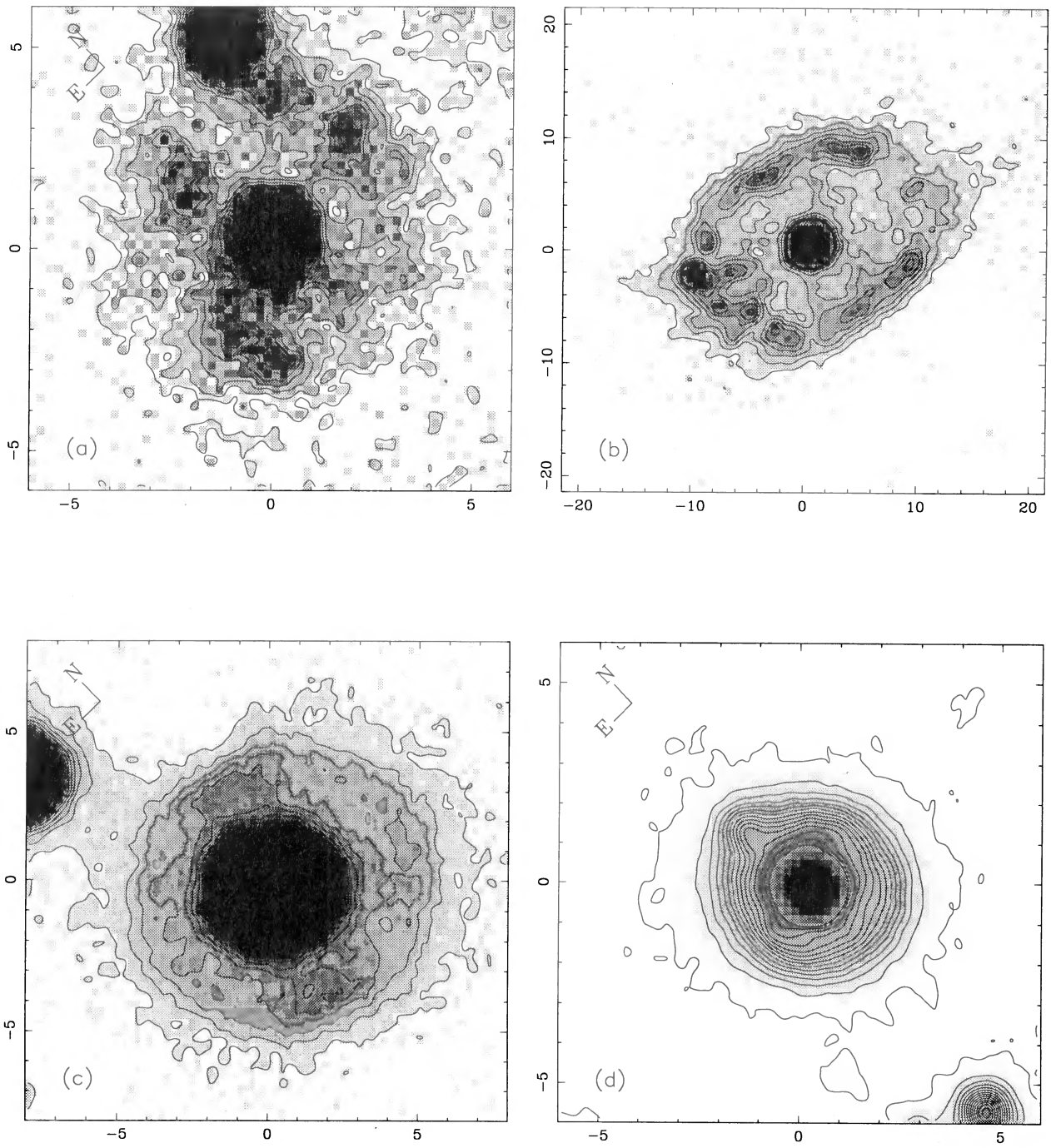

Figure 6. In all four plots axes are marked in arcsec and the bottom contour is set at 2σ above the background: (a) Hα, band 6, image of the remnant of V1500 Cyg, frame orientation is as indicated on the plot and the contours are separated by 1σ (see Section 3.5); (b) Hα, band 5, image of the remnant of T Aur, north is up, east is to the left, 2σ contour intervals (Section 3.6); (c) band 6 image of the remnant of V533 Her, orientation as indicated, 2.5σ contour intervals (Section 3.7); (d) band 6 image of the remnant of NQ Vul, orientation as indicated, 7σ contour intervals (Section 3.8).

3.6 T Aurigae

3.6.1 Background

T Aur (Nova Aurigae 1891) is often referred to as the twin of DQ Her because of their similar outburst characteristics and light curves. After reaching a maximum photographic magnitude of 4.1, T Aur declined at a moderately high rate, with a t_3 of 100 d. The quiescent minimum visual magnitude is 14.9. The best published image to date (Gallagher et al. 1980) appeared to have the same basic structure as that of DQ Her, a filled inhomogeneous, elliptical ring with the possibility of equatorial/tropical bands, although the shell of T Aur appears to be much smaller with a lower surface brightness. T Aur is known to be an eclipsing binary with an

angle of inclination $\simeq 57°$ (Ritter 1984) or 68° (Bianchini 1980). Duerbeck (1981) quotes a distance of 600 pc.

3.6.2 Results

The remnant of T Aur in band 5 is shown in Fig. 6(b). The co-added image was produced by observing the object for a total of 1320 s over two exposures. The very low-level features in this image should be viewed with caution as the CCD fringing proved difficult to remove completely. The oval remnant has overall dimensions of approximately 30×20 arcsec^2, the major axis lying at PA 147°, whilst the bright shell itself extends to about 22×16 arcsec^2. The emission in the south-east of the shell forms a thick cap comprising at least four distinct clumps. These clumps are elongated about the direction of the major axis and appear to form 'tails' at their outermost extent similar to those seen in DQ Her (Fig. 1d). In contrast, the emission in the north-west is diffuse with little apparent structure. Slices across the nebula show that the central region of faint nebulosity is inhomogeneous with several blobs and bands of enhanced emission.

3.6.3 Interpretation

From the image in Fig. 6(b) it is clear that the similarities between T Aur and DQ Her extend to the structure of their remnants. It is likely that the similarities are a result of the same dynamical processes operating at outburst and beyond. Differences between the two nebulae may well be the result of the additional 40-yr evolution in the case of T Aur.

3.7 V533 Herculis

3.7.1 Background

V533 Her (Nova Herculis 1963) reached a maximum photographic magnitude of 3.0 before declining at a moderately high rate, with a t_3 of 44 d. It has a minimum visual magnitude of 15.6. After an unsuccessful search by Wray (private communication to Patterson 1979), a nebular remnant was first discovered by CR83. By comparing the nova profile with that of a nearby field star the radius was estimated to be 1.6 arcsec in 1983 and 3.5 arcsec in 1985 (C85). Note that these radii compared with our estimated dimensions (see below) suggest that the 1983 measurement may be in error. There is also some evidence to suggest that, like DQ Her, V533 Her contains a strongly magnetized white dwarf (Patterson 1979; although see Robinson & Nather 1983). Warner (1986) estimates an orbital inclination of $\sim 62°$ on the basis of the width of emission lines assumed to arise from the accretion disc. Duerbeck (1981) quotes a distance of 680 ± 250 pc.

3.7.2 Results

The image of V533 Her, Fig. 6(c), was produced by co-adding two 900-s exposures through the band 6 Hα filter. The remnant consists of an approximately circular nebula of diffuse emission. There is a 1.5 arcsec wide bar extending across the nebula with PA $\sim 160°$. The ends of the bar appear to be limb-brightened. Eight slices across the remnant suggest that the nebula consists of a fairly homogeneous ring, filled with diffuse emission, with few obvious features other than the bar. The radius of the ring is on average about 4.5 arcsec, although the radius of the eastern half is ~ 0.5 arcsec smaller than that of the western half.

3.7.3 Interpretation

The remnant of V533 Her appears to be another example of the ellipsoidal shell/equatorial ring morphology evident in the remnant of FH Ser. If this model is correct then the bar of enhanced emission is identified as the equatorial ring. Given that the enhanced band appears to pass directly across the central object, this suggests that the central binary should be eclipsing. It is easy to demonstrate, however, that morphologies of the type seen here can be produced with a large range of inclination angles, provided that the observed equatorial band is fairly broad as it appears to be in this case. There is no evidence in the literature indicating an eclipsing central system. The slight elongation of the western hemisphere is probably the result of ghosting, as field stars also show similar low-level emission.

3.8 NQ Vulpeculae

3.8.1 Background

From a photographic minimum of 18.3, NQ Vul (Nova Vulpeculae 1976) outburst to reach a maximum visual magnitude of 6.1. The decline is defined as moderately fast with a t_3 of 65 d. It has also been classed as a DQ Her-type nova because of a deep trough in the light curve beginning approximately 60 d after the peak. Duerbeck (1981) quotes a distance of 1200 pc.

3.8.2 Results

The Hα band 6 image of NQ Vul, Fig. 6(d), was obtained by co-adding two 900-s exposures. The remnant, detected here for the first time, consists of a central object sitting on a pedestal of emission which fades with increasing radius. Slices across the nebula suggest that the remnant extends out to an average radius of ~ 4 arcsec. All the slices have large shoulders of emission at a radius of ~ 1.5 arcsec, with an intensity ~ 20 per cent of the central peak intensity. There appears to be some barely resolved structure in the western hemisphere of the remnant. The contours also suggest that, apart from the knot of brighter emission to the north, there is a bar-like feature in the underlying emission extending across the central object at a PA of $\sim 140°$.

3.8.3 Interpretation

MEM deconvolution and slices across the image suggest that the remnant comprises a complete homogeneous circular ring with a radius of approximately 1.5 arcsec and a width of approximately 0.5 arcsec. It also seems that the bright knot directly north of the central object is unassociated with the nova and is therefore probably a field star. The MEM results also suggest that the underlying asymmetry mentioned in the previous section is not connected with the field star and that the western half of the remnant does appear to have a greater surface brightness than the rest of the remnant. This may be an intrinsic property of the shell or it may be a natural

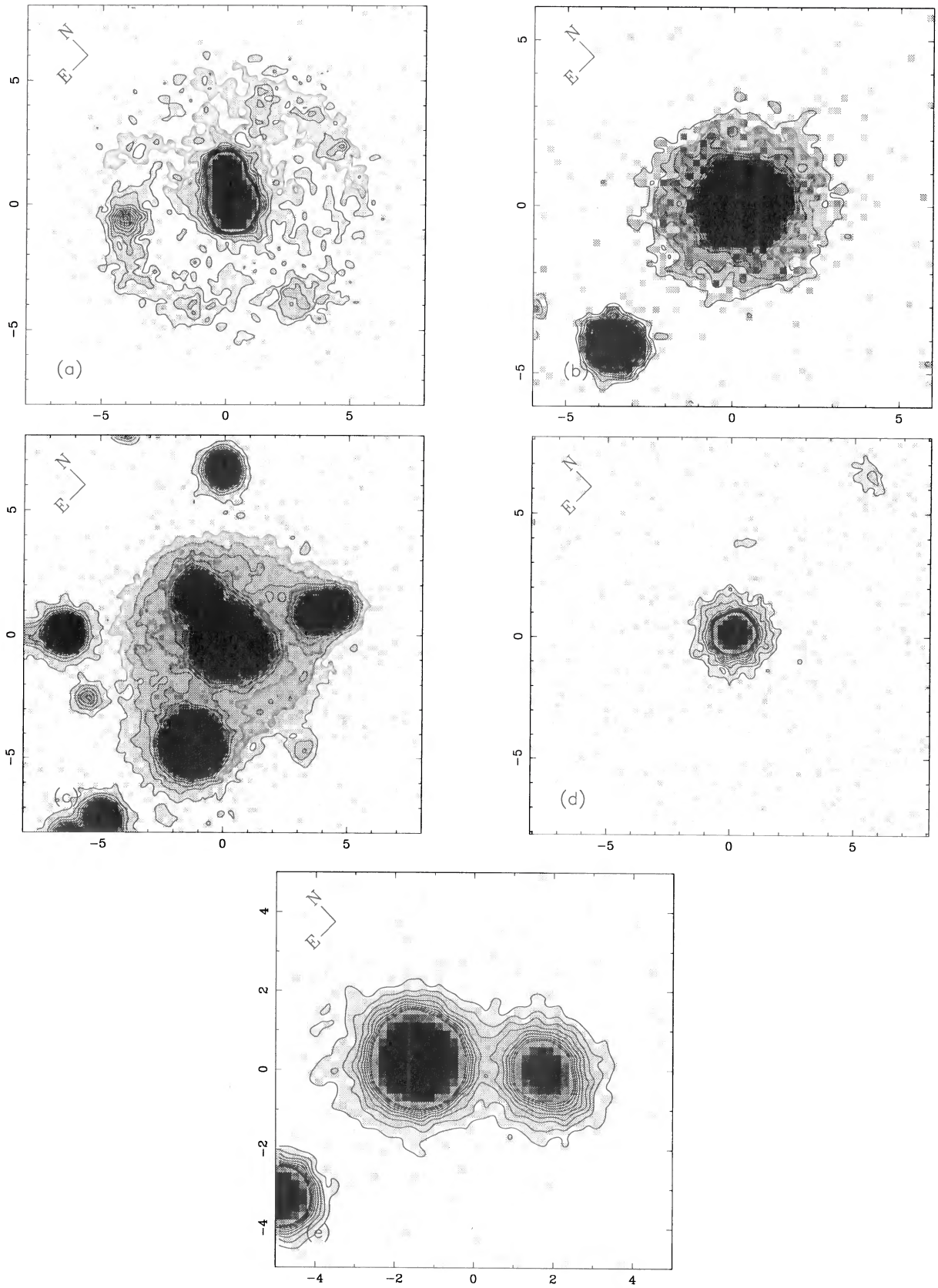

Figure 7. In each of the above CCD images the orientation of the frames with respect to the sky is indicated on the plot, the bottom contour level is set at 2σ above the background, and axes are marked in arcsec. All images are made using the band 6 (Hα, 6569-Å effective central wavelength) filter: (a) V476 Cyg, 1σ contour intervals (Section 3.9); (b) DK Lac, 1σ contour intervals (Section 3.10); (c) LV Vul, 2σ contour intervals (Section 3.11); (d) RW UMi, 1σ contour intervals (Section 3.12); (e) V450 Cyg (right-hand object on frame), 1.5σ intervals (Section 3.13).

consequence of the Hα filter being offset from the rest wavelength by 3 Å, equivalent to a velocity shift of ~ 140 km s^{-1}. The surface brightness enhancement could then be a result of the western half of the remnant being tilted towards the observer. Seen in the context of better-resolved features in the remnants previously discussed, the bar may indicate the presence of some form of equatorial ring.

3.9 V476 Cygni

3.9.1 Background

V476 Cyg (Nova Cygni 1920) reached a maximum magnitude of 2.0 from a quiescent visual magnitude of 17.1. The outburst declined with a t_3 of 16 d and is classified as very fast. Noteworthy features in the spectral development of the outburst included the complexity of the absorption lines, with at least 12 distinct systems (Payne-Gaposchkin 1957). CR83 observed the shell in 1981 and determined its radius to be 5.7 arcsec. The previously published image of this nova (Duerbeck 1987a) showed a very faint shell with a diameter of about 5.6 arcsec in 1984. A distance of 1500 pc was derived.

3.9.2 Results

The image of V476 Cyg, Fig. 7(a), was obtained with a 900-s exposure through the band 6 Hα filter. The remnant consists of an inhomogeneous circular region of diffuse emission, with at least six knots of enhanced emission at approximate position angles 49°, 107°, 164°, 250°, 266° and 296°. The nebula appears remarkably similar to the remnant of V1500 Cyg, Fig. 6(a). Slices across the remnant suggest that the circular nebula has a radius of about 5.5 arcsec. The brightest knot, at a PA of $\sim 45°$, is about a tenth of the brightness of the central star. It is likely that the apparent elongation of the central source in the north-western direction is due to the presence of a field star 1.5 arcsec from the main central object.

3.9.3 Interpretation

Previous images of the remnant of V476 Cyg (for example, Duerbeck 1987a) have been too indistinct to extract any information apart from the extent and hence, via expansion parallax, an estimate of the distance. It is not clear therefore whether the knots of emission we have detected formed at outburst or some time later, although the complexity of the early spectra indicate that the former is more likely to be the case. Five of the knots seen in the image in Fig. 7(a) lie on opposite sides of the central object in two groups and may constitute a band of enhanced emission, running along the east–west axis, similar to that seen in V533 Her. A slice taken across the bright knot at PA 49° does not rule out the possibility that the feature may be stellar in origin. This might also explain its relative brightness with respect to the other knots and raise doubts about the presence of an east–west band. The diffuse remnant appears approximately circular, suggesting that the outburst itself was spherically symmetric, although the ejecta themselves were clumpy.

3.10 DK Lacertae

3.10.1 Background

DK Lac (Nova Lacertae 1950) was discovered in 1950 January on its rise from a quiescent magnitude of 15.5 to peak at 5.9, both of these values being derived from photographic photometry. The moderately fast decline was characterized by a t_3 of 32 d and unusually large fluctuations which persisted while the underlying light curve declined by several magnitudes. In C85 the remnant was 'marginally' detected, by stellar-profile comparison, with an estimated radius of 2.0 arcsec. C85 also quotes an expansion velocity of 1075 km s^{-1}. Duerbeck (1981) estimates a distance of 1500 ± 200 pc.

3.10.2 Results

The 900-s band 6 image of DK Lac is shown in Fig. 7(b). The extended emission is dominated by the central object. Slices across the remnant show shoulders of emission at a radius averaging ~ 2.5 arcsec. A slice along the north–south axis shows shoulders of emission at radii of ~ 2.0 arcsec.

3.10.3 Interpretation

It is tempting to suggest that the north–south axis of the remnant of DK Lac represents a region of enhanced emission similar to those associated with equatorial bands seen in other objects. The brightness of the central object, however, relative to the nebular emission and the errors associated with measuring the position and brightness of individual features necessitate caution.

3.11 LV Vulpeculae

3.11.1 Background

LV Vul (Nova Vulpeculae 1968 No. 1) peaked at a maximum visual magnitude of 5.17 from a quiescent photographic magnitude of 16.9. The outburst declined with a t_3 of 37 d and is classed as a fast nova. From spectroscopic observations Sobotka, Stefl & Grygar (1977) obtained an average expansion velocity of 1700 ± 300 km s^{-1}, estimated a distance of 1450 ± 400 pc, and predicted that the nebular diameter at that time should have been close to 4.0 arcsec. C85 resolved a shell for the first time and by stellar-profile comparison and radial-profile fitting adopted a shell diameter of 5.6 arcsec.

3.11.2 Results

The image of LV Vul, Fig. 7(c), was obtained with a 900-s exposure through the Hα filter in band 6. Any structure within the remnant is probably obscured by the presence of field stars. Slices across the nebula tentatively suggest that the shell has a radius of ~ 5 arcsec. The remnant is not sufficiently resolved to allow detailed interpretation although the emission appears to be approximately circularly symmetric.

3.12 RW Ursa Minoris

3.12.1 Background

RW UMi (Nova Ursa Minoris 1956) is a very poorly studied nova for which little information is available in the literature. The nova brightened from a quiescent photographic magnitude of 21 to a photographic peak of 6. It declined with a t_3 of 140 d and is noteworthy as a nova with a high galactic latitude.

3.12.2 Results

This Hα observation, shown in Fig. 7(d), had the shortest integration time of all our nova images with a 600-s exposure in band 6. The remnant consists of a bright central object surrounded by a diffuse region of material. Comparison with a field star on the frame shows that this emission does not arise from the wings of the PSF of the central star. Slices across the frame suggest that the bulk of the emission is concentrated in a ring at a radius of ~ 1.5 arcsec. MEM deconvolution confirms this, revealing a ring of inhomogeneous material. There are two regions of nebulous emission close to the main object but unconnected to the bulk of the nebula. The fainter of the two is ~ 3 arcsec north-west of the star while the brighter, more extended region is ~ 8 arcsec directly west. It is not clear whether these two regions are real or physically associated with the remnant.

3.13 V450 Cygni

3.13.1 Background

V450 Cyg (Nova Cygni 1942) outburst from a quiescent photographic magnitude of approximately 16 and is thought to have peaked at a magnitude of around 7.0. Maximum light was not actually observed as the nova was discovered as an eighth-magnitude star 3 months after the estimated peak. The decline is classified as slow with a t_3 of 108 d (Duerbeck 1987b), although this estimate clearly has to be treated with some caution. The light curve, like that of DQ Her, exhibits large fluctuations at maximum and a deep minimum. The spectral development of the nova is also very similar to that of DQ Her (Sanford 1942). During her survey in 1983/1984, Cohen (1985) was unable to detect a shell for this object. Duerbeck (1987b) quotes a distance of 1800 ± 400 pc.

3.13.2 Results

The image of V450 Cyg is shown in Fig. 7(e) and is the result of a 1200-s exposure through the Hα filter. V450 Cyg is the object south-west of the brightest object on the frame, a field star. It is immediately apparent that the nova is extended because the two PSFs, as measured by the lowest contour plotted, are of comparable size yet the field star is much brighter. Slices along PA 45° and 135° show two shoulders of emission either side of the central object, the former at a radius of about 1.2 arcsec, the latter at 1.8 arcsec. There is a high degree of symmetry about these axes. Slices along the major axis oriented at PA $\sim 170°$ show that the nebula extends out to a minimum discernible diameter of approximately 4.5 arcsec, in contrast to the minor axis where the diameter is only 3 arcsec.

4 ANALYSIS

4.1 A link between speed class and shaping?

The images presented in the previous section suggest that the remnants can be classified into two broad groups defined by the speed class of the nova (its rate of decline from optical maximum). In particular, the slower novae (in our sample DQ Her, HR Del, FH Ser, T Aur, V533 Her and V450 Cyg; RR Pic is a similar case, see Evans et al. 1992) tend to produce structured remnants which are often loosely described as having 'polar blobs/equatorial ring morphologies'. In contrast, the faster novae (GK Per, V476 Cyg and V1500 Cyg; CP Pup is probably another example, see Williams 1982) produce apparently inhomogeneous, approximately circular, shells with discrete randomly distributed knots of brighter emission.

Fig. 8 shows a graph of axial ratio (the ratio of the lengths of the major and minor axes of the nova shell) against nova speed class (the t_3 time). A moment analysis was performed on each of the nova remnants, allowing automated determination of the axial ratio for most of the objects. For the images in which field stars interfere with a rigorous moment analysis the aspect ratios were determined by analysing slices across the remnants. Aspect ratios for CP Pup and RR Pic were obtained by examining the images published by Williams (1982) and Evans et al. (1992).

These data represent strong evidence for the existence of a correlation between the aspect ratio of the remnant and the t_3 time of the nova. In fact, a Spearman rank-order correlation test suggests that the raw observed data (the open circles on Fig. 8) are correlated at the 99 per cent confidence level. There are several reasons, however, why this correlation may intrinsically be even stronger. For example, interaction with an inhomogeneous ambient medium could distort the shell (as for GK Per perhaps), whilst orientation will cause the points to scatter such that the intrinsic correlation will be represented by the upper envelope of the points in Fig. 8. For those novae where estimates of the angle of inclination have been made [DQ Her and FH Ser from our observations; GK Per, HR Del, T Aur and V533 Her are quoted in the literature – see Section 3; we estimated the inclination of RR Pic to be $68° \pm 10°$ from examination of an apparent ring on the image published by Duerbeck (1987c), although Warner (1986) suggests that the inclination is 80°], we have deprojected the observed aspect ratio and have plotted the resulting estimate of the true aspect ratio of the remnant. We plot multiple points where more than one estimate of the inclination exists.

The data plotted in Fig. 8, although representing a statistically significant correlation, are not sufficient to determine the exact form of this correlation. In addition, systematic errors in our estimates of axial ratio are likely to yield underestimates of the inclinations. We have illustrated this latter point by including in Fig. 8 measurements of the axial ratio for HR Del from the narrow-band Hα band 5 image, a composite broader-band Hα image formed from a sum of the band 3, 4, 5 and 7 images, and a measurement from the band 9 [O III] image. The first two show that the band 5 measurements may well underestimate aspect ratios for those shells that are seen at relatively small inclination angles by not revealing higher velocity features at the extremes of the major axis. Although the [O III] measurement continues

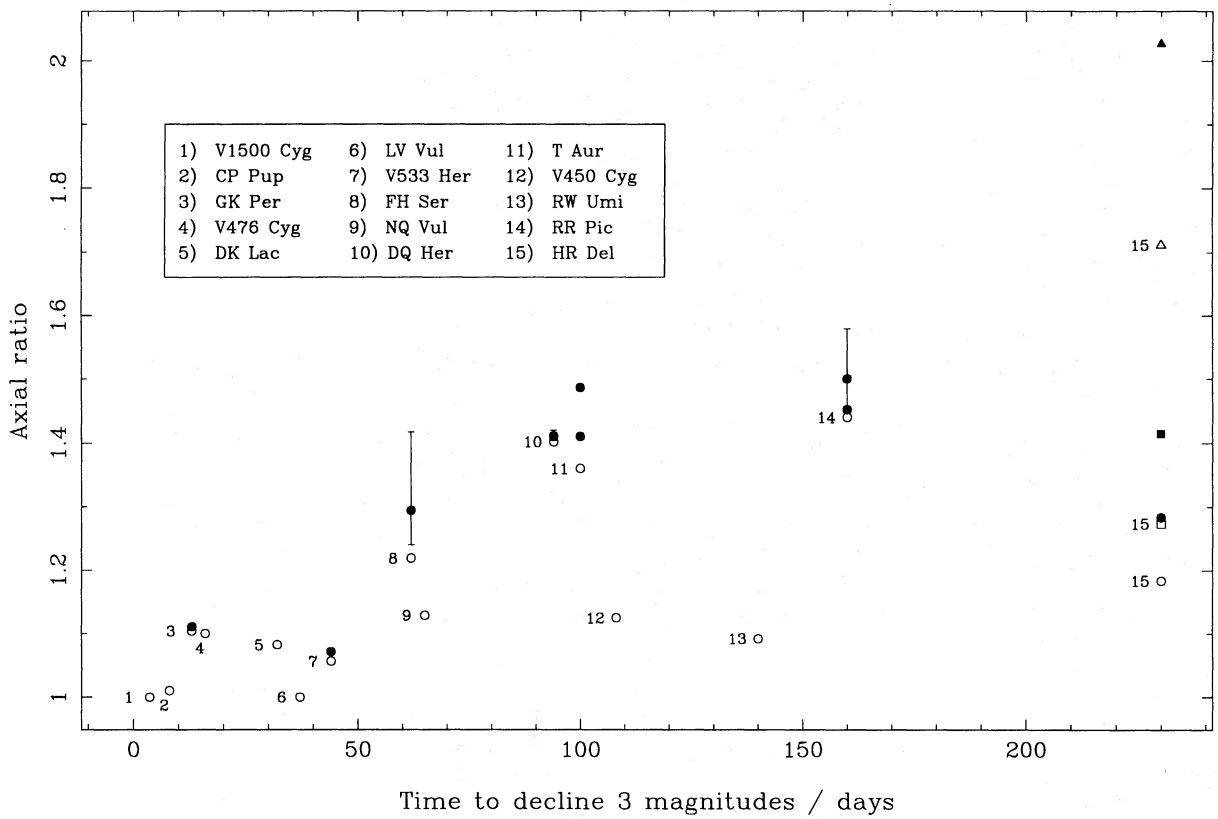

Figure 8. Plot of the axial ratio of the nova shells versus speed class in terms of t_3, the time taken for the optical light curve to drop by 3 mag. The observed axial ratios are marked with open symbols. For those novae with known or estimated orbital inclinations we have deprojected the observed aspect ratio and also plot the intrinsic aspect ratio (marked with filled symbols). Circular symbols represent measurements made from the band 5 or band 6 Hα images, apart from CP Pup and RR Pic which are measured from images published by Williams (1982), Evans et al. (1992) and Duerbeck (1987c). In the case of HR Del we present a further two measurements (see text): the open square represents a measurement made from a composite broader band Hα image composed of a sum of the band 3, 4, 5 and 7 images; whilst the open triangle is measured from the band 9 [O III] image.

this trend, the issue is rather more complicated in this case because the morphology is likely to be emission-line-dependent (for example, see Duerbeck 1987c). A further effect which leads to underestimates of axial ratio is the contribution of light from the central object. In objects that are poorly resolved (because they are younger, or are more distant, or contain an intrinsically bright central system), the effect of the PSF is always to circularize any extended emission. This is likely to affect our observations of HR Del, V533 Her, NQ Vul, DK Lac, RW Umi and V450 Cyg.

The physical reason for a connection between speed class and shaping may lie in the common-envelope phase thought to occur in the outbursts of most classical novae, and during which angular momentum is removed from the binary system (Shankar, Livio & Truran 1991; Iben & Livio 1993). The remnants of slower novae which spend a greater length of time in a common envelope will be affected more by the orbital motions of the binary system than faster novae which spend only a short time in a common envelope. Although the role of the common-envelope phase in shaping planetary nebulae has received much attention, only 15 or so of these objects are known to have binary nuclei, and their common-envelope phase is likely to have ended thousands of years ago (Bond 1989; Iben & Livio 1993). This can be contrasted with classical novae, in which the majority of objects undergo a common-envelope phase that can be observed as it takes place, and the effects of which on the remnant can be investigated only a few years later. Similar common-envelope or interacting winds mechanisms are likely to be responsible for features observed in radio VLBI maps (Pavelin et al. 1993) and *Hubble Space Telescope* images of the remnant of Nova Cygni 1992 (Paresce 1994), and for the rings seen in *HST* observations of SN1987a (Panagia et al. 1991). In fact it is intriguing to note that the latest *HST* images of SN1987a (Burrows et al. 1995) show three rings of emission oriented in a similar fashion to the three rings we see in our observations of DQ Her; it seems possible that similar physical processes are operating (Lloyd, O'Brien & Kahn 1995; section 5).

It should be noted however, that, although the common-envelope phase is an attractive shaping mechanism for classical nova shells, one might also expect other mechanisms, for example the effects of white dwarf rotation, to be less efficient for faster mass ejection.

4.2 Distance determination

Nebular expansion parallax provides us with, in principle, one of the most accurate methods of distance determination.

Inaccuracies, however, can arise from three sources: (i) determination of the expansion velocity; (ii) association of this expansion velocity with components seen in images of the remnant; and (iii) changes in the expansion velocity since outburst, for example as a result of sweeping up some ambient medium.

In Table 2 we list distance estimates for all 13 novae. Expansion velocities are taken from the literature, whilst the position of material presumed to be moving at this velocity is determined from the limb-brightened rings seen in our images. These rings must be in the plane of the sky and will thus be a more reliable feature to measure than the bright knots, which in principle could be moving at any angle to the line of sight. An alternative approach is to assume that individual knots, in an object like V1500 Cyg for example (see Fig. 6a), are all moving at the same intrinsic speed but in different directions, as suggested by Hack et al. (1993). This implies that some time after outburst they will be scattered at various distances from the central object. It is possible, however, to associate individual knots with peaks in the high-resolution spectra because it is clear that the knot closest to the central object, for example, will have the highest line-of-sight velocity. Knots can then be ranked in terms of their distance from the centre and their radial velocities determined from the spectrum. It is then a simple task to vary the assumed ejection speed (common to all the knots) and the angle of ejection to the line of sight (unique to each knot) and minimize the resulting discrepancies between the observed knot positions and the model positions. In the case of V1500 Cyg, for which a suitable spectrum is available (Hutchings & McCall 1977), this procedure leads us to estimate a distance of 1550 pc with a knot ejection speed of 1480 km s^{-1}.

The discussion of shaping in the previous section leads us to suggest that, where distance estimates are required for calibration of the maximum-magnitude–rate-of-decline relationship (C85; Livio 1992), for example, it is better to use the faster novae whose outbursts are more likely to be spherical and whose distances determined by expansion parallax are therefore more reliable.

Table 2. Distance estimates by nebular expansion parallax. Notes. (1) The velocity is taken from CR83; error estimate from the ellipticity of the remnant. Inclination angles for DQ Her and T Aur taken to be 81° (Section 3.1.4) and 57° (Ritter 1984) respectively. (2) Again, the velocity is from CR83, the ring is assumed to be limb-brightened and the error arises in an estimated 0.5-arcsec error in its position. (3) Expansion velocities derived directly from [O III] spectra published by Solf (1983). The errors are associated with the width of the spectral features. (4) The velocity from CR83 is assumed to be in the plane of the sky; expansion along the minor axis is not considered because strong interaction and hence retardation have occurred; the error is obtained by assuming a 4-arcsec error in measuring the exact location of the limb-brightened shell. (5) The velocity is from C85; the ring is assumed to be limb-brightened; the error is from an estimated 0.5-arcsec error in ring position. (6) The velocity is from Payne-Gaposchkin (1957), the ring is assumed to be limb-brightened, and the error is estimated from a 0.5-arcsec uncertainty in the ring position.

Object	Expansion velocity (km s^{-1})	Distance (pc)	Notes
DQ Her	315	400±60	1
FH Ser	560	920±130	2
HR Del	560	760±130	3
GK Per	1200	455±30	4
V1500 Cyg	1180	1500±200	2
T Aur	655	960± 220	1
V533 Her	580	560±70	2
NQ Vul	705	1600±800	2
V476 Cyg	790	1620±120	2
LV Vul	860	920±80	5
RW UMi	950	5000±2000	2
DK Lac	1075	3900±500	2
V450 Cyg	500	3500±800	6

5 SUMMARY

From the 13 new, deep images of old classical nova remnants presented in this paper, we have been able to draw the following conclusions.

(i) A correlation exists between speed class and the shape of nova shells. This suggests that fast novae produce spherical remnants consisting of knots of enhanced emission, the distribution of which appears almost random, superposed on rather more diffuse emission. In contrast, slower novae produce ellipsoidal remnants that are structured, containing equatorial and tropical rings, and polar blobs.

(ii) New distance estimates for the 13 novae have been derived via expansion parallax.

(iii) The orientation of equatorial rings can be used to determine orbital inclinations of nova systems: for example, we estimate inclinations of 81°±4° for DQ Her, and 58°±14° for FH Ser.

(iv) The remnant of DQ Her is an ellipsoidal shell constricted by three rings – recent numerical calculations (see, for example, O'Brien, Lloyd & Slavin 1995) suggest that the tropical rings may be formed as a result of sweeping up conical regions of enhanced density in the mass ejected from the white dwarf; the cones are produced as a result of the frictional interaction of the main-sequence binary companion with the wind.

(v) For DQ Her, a faint halo extends out to almost twice the size of the previously known bright shell. This halo contains symmetrically distributed long tails originating in bright knots within the shell; similar features are also seen in our images of the remnant of T Aur and previous images of RR Pic.

(vi) We suggest that a new region of interaction has developed in the north-eastern quadrant of GK Per. Emission in the south-eastern quadrant appears to have formed a 'blister' on the main shell and there is some indication that at one point on the shell ejecta have blown out into a lower-density environment.

(vii) We have detected and resolved the nebular remnants of novae V450 Cyg and NQ Vul. The former is elliptical with approximate dimensions of $\sim 4.5 \times 3.0$ arcsec^2, whilst the latter appears circular with radius 1.5 arcsec.

(viii) We have resolved structure in the remnants of FH Ser and V533 Her, indicating that they comprise ellipsoidal shells with equatorial rings of enhanced emission.

(ix) Sub-arcsecond seeing conditions have allowed confirmation of the detailed structure of the remnant of HR Del suggested by the results of our previously published image restoration. In particular, the remnant appears to possess an

equatorial ring together with polar blobs which may represent the limb-brightened extrema of tropical rings, similar to those seen in our images of DQ Her and published images of RR Pic (e.g. Evans et al. 1992).

(x) The remnants of V1500 Cyg and V476 Cyg have been resolved into circularly symmetric diffuse shells with several, typically four to six, clumps of enhanced emission.

ACKNOWLEDGMENTS

AJS acknowledges the PPARC for receipt of a studentship and travel funding. We thank Héctor Castañeda and Nic Walton for their support during the observing run. Data reduction and analysis were performed using the Liverpool John Moores University Starlink node. This paper is based on observations made with the WHT and the JKT, operated by the Royal Observatories on La Palma, Canary Islands.

REFERENCES

Baade W., 1940, PASP, 52, 386
Becker H. J., Duerbeck H. W., 1980, PASP, 92, 792
Bianchini A., 1980, MNRAS, 192, 127
Bianchini A., Sabbadin F., 1983, A&A, 125, 112
Bode M. F., Evans A., 1989, Classical Novae. Wiley & Sons Ltd, Chichester
Bode M. F., Seaquist E R., Evans A., 1987, MNRAS, 228, 217
Bond H. E., 1989, in Torres-Peimbert S., ed., Proc. IAU Symp. 131, Planetary Nebulae. Kluwer, Dordrecht, p. 251
Burrows C. J. et al., 1995, ApJ, in press
Cohen J. G., 1985, ApJ, 292, 90 (C85)
Cohen J. G., Rosenthal J., 1983, ApJ, 268, 689 (CR83)
Duerbeck H. W., 1981, PASP, 93, 552
Duerbeck H. W., 1987a, Ap&SS, 131, 461
Duerbeck H. W., 1987b, Space Sci. Rev., Vol. 45, Nos 1–2
Duerbeck H. W., 1987c, ESO Messenger, 50, 9
Duerbeck H. W., 1992, Acta Astron., 42, 85
Dyson J. E., Hartquist T. W., Biro S., 1993, MNRAS, 261, 430
Evans A., Bode M. F., Duerbeck H. W., Seitter W. C., 1992, MNRAS, 258, 7P
Friedjung M., 1989, in Bode M. F., Evans A., eds, Classical Novae. Wiley & Sons Ltd, Chichester, p. 187
Gallagher J. S., Hedge E. K., Kopriva D. A., Williams R. E., Butcher H. R., 1980, ApJ, 237, 55
Hack M., Selvelli P. L., Bianchini A., Duerbeck H. W., 1993, in Hack M., la Dous C., eds, Cataclysmic Variables and Related Objects. US Govt Printing Office, Washington, p. 413
Hutchings J. B., 1972, MNRAS, 158, 177
Hutchings J. B., McCall M. L., 1977, ApJ, 217, 775
Iben I., Livio M., 1993, PASP, 105, 1373
Ivison R. J., Hughes D. H., Lloyd H. M., Bang M. K., Bode M. F., 1993, MNRAS, 263, L43
Kohoutek L., 1981, MNRAS, 196, 87P
Lamb D. Q., Patterson J., 1983, in Livio M., Shaviv G., eds, Cataclysmic Variables and Related Objects. Reidel, Dordrecht, p. 229
Livio M., 1992, ApJ, 393, 516
Lloyd H. M., O'Brien T. J., Bode M. F., Predehl P., Schmitt J. H. M. M., Trümper J., Watson M. G., Pounds K. A., 1992, Nat, 356, 222
Lloyd H. M., Bode M. F., O'Brien T. J., Kahn F. D., 1993, MNRAS, 265, 457
Lloyd H. M., O'Brien T. J., Kahn F. D., 1995, MNRAS, 273, L19
McLaughlin D. B., 1960, in Greenstein J. L., ed., Stars and Stellar Systems, Vol. 6. Univ. Chicago Press, Chicago, p. 585
Martin P. G., 1989, in Bode M. F., Evans A., eds, Classical Novae. Wiley & Sons Ltd, Chichester, p. 93
O'Brien T. J., Bode M. F., Kahn F. D., 1992, MNRAS, 255, 683
O'Brien T. J., Lloyd H. M., Bode M. F., 1994, MNRAS, 271, 155
O'Brien T. J., Lloyd H. M., Slavin A. J., 1995, in Harpaz A., Soker N., eds, Asymmetrical Planetary Nebulae. Ann. Israel Phys. Soc., Vol. 11, Institute of Physics, Bristol, p. 258
Panagia N., Gilmozzi R., Macchetto F., Adorf H.-M., Kirshner R. P., 1991, ApJ, 380, L23
Paresce F., 1993, in Errico L., Vittone A. A., eds, Stellar Jets and Bipolar Outflows. Kluwer, Dordrecht, p. 127
Paresce F., 1994, A&A, 283, L3
Patterson J., 1979, ApJ, 233, L13
Pavelin P. E., Davis R. J., Morrison L. V., Bode M. F., Ivison R. J., 1993, Nat, 363, 424
Payne-Gaposchkin C., 1957, The Galactic Novae. Dover Publications Inc., New York
Perrine C. D., 1902, ApJ, 14, 249
Ritter H., 1984, A&AS, 57, 385
Robinson E. L., Nather R. E., 1983, ApJ, 273, 255
Sanford R. F., 1942, PASP, 55, 196
Seaquist E. R., Bode M. F., Frail D. A., Roberts J. A., Evans A., Albinson J. S., 1989, ApJ, 344, 805
Shankar A., Livio M., Truran J. W., 1991, ApJ, 374, 623
Slavin A. J., O'Brien T. J., Dunlop J. S., 1994, MNRAS, 266, L55 (SOD94)
Sobotka M., Stefl S., Grygar J., 1977, in Friedjung M., ed., Novae and Related Stars. Reidel, Dordrecht, p. 96
Solf J., 1983, ApJ, 273, 647
Stockman H. S., Schmidt G. D., Lamb D. Q., 1988, ApJ, 332, 282
Unger S. W., Brinks E., Laing R. A., Tritton K. P., Gray P. M., 1988, Observers Guide Version 2. Isaac Newton Group, Royal Greenwich Observatory, Cambridge
Unger S. W., Taylor K., Pedlar A., Ghataure H. S., Penston M. V., Robinson A., 1990, MNRAS, 242, 33P
Wade R. A., 1990, in Cassatella A., Viotti R., eds, Proc. IAU Colloq. 122, Physics of Classical Novae. Springer-Verlag, Berlin, p. 179
Wade R. A., Ciardullo R., DeVeny J. B., Jacoby G. H., Schoening W. E., 1990, in Cassatella A., Viotti R., eds, Proc. IAU Colloq. 122, Physics of Classical Novae. Springer-Verlag, Berlin, p. 195
Walker M. F., 1956, ApJ, 123, 68
Warner B., 1986, MNRAS, 222, 11
Williams R. E., 1982, ApJ, 261, 170